Electron knock-on cross section of carbon and boron nitride nanotubes

A. Zobelli,[1,2,*] A. Gloter,[1] C. P. Ewels,[3] G. Seifert,[2] and C. Colliex[1]
[1]*Laboratoire de Physique des Solides, CNRS, UMR 8502, Université Paris-Sud, F-91405 Orsay Cedex, France*
[2]*Institüt für Physikalische Chemie und Elektrochemie, Technische Universität Dresden, D-1062 Dresden, Germany*
[3]*CNRS UMR 6502, Institute des Materiaux, 2 Rue de la Houssiniere, 44322 Nantes, France*
(Received 5 February 2007; published 5 June 2007)

We present a theoretical description of electron irradiation of single-walled carbon and boron nitride nanotubes. In a first step, the anisotropy of the atomic emission energy threshold is obtained within extended molecular-dynamics simulations based on the density-functional tight-binding method. In a second step, we numerically derive the total Mott cross section for different emission sites as a function of the incident electron energy. Two regimes are then described: at low irradiation energies (below 300 keV), the atoms are preferentially ejected from the upper and lower parts of the tube, while at high energies (above 300 keV), the atoms are preferentially ejected from the side walls. Typical values from a fraction of barn (at side wall for 150 keV electron) up to around 20 barn (for 1 MeV electrons) are obtained for the total cross section of knock-on processes for both C and BN nanotubes. These values are smaller than those previously reported using isotropic models and the main reasons for the discrepancies are discussed. Finally, in boron nitride nanotubes, we report that the emission energy threshold maps show boron sputtering to be more favorable for low irradiation energies, while nitrogen sputtering is more favorable at high energies. These calculations of the total knock-on cross section for various nanotubes can be used as a guideline for transmission electron microscopy experimentalists using high energy focused beams to shape nanotubes, and also more generally if electron irradiation is to be used to change nanotube properties such as their optical behavior or conductivity.

DOI: 10.1103/PhysRevB.75.245402 PACS number(s): 61.46.Fg, 61.80.−x, 61.80.Az

I. INTRODUCTION

The influence of defects on the mechanical, chemical, and electronic properties of organic and inorganic nanotubes has been underlined in recent years by a large number of studies.[1–3] Transmission electron microscopy (TEM) appears to be a suitable technique for studying defects in carbon nanotubes. Recent improvement in TEM techniques has shown the possibility of direct imaging of single defective structures in single-walled nanotubes[4,5] and of monitoring their evolution over time under homogeneous irradiation.[6]

Electron bombardment presents three main advantages due to the low-energy transmitted between the incident electron and the knocked atom. First, the transfer of energy and the irradiation dose can be so low that in a first approximation only individual defects are generated. Second, the energy of the incident electron can be finely tuned around the threshold value where defects can just be created. Finally, electron beams in a TEM can be focused to form a nanometric probe, allowing control of the irradiated area with high spatial resolution.[7] Compared to other irradiation methods electron irradiation presents the additional advantage that defect production can be easily observed and controlled *in situ*.

In this context, a correct derivation of the sputtering cross section and subsequently of the emission probability could bring important new insights for the design and interpretation of future experiments. Total knock-on cross sections for carbon atoms in nanosystems have already been derived under the hypothesis that atoms lie in an isotropic potential well.[8] However, the strong anisotropy of nanotubular systems requires us to go beyond this simple approximation. In their work, Crespi *et al.*[9] reported several values of the escape threshold energy as a function of the direction of the kinetic energy of the escaping carbon atom. A threshold energy at around 17 eV was estimated for the radial escaping direction while energies of approximately 40 eV were obtained for tangential ejection. Nevertheless, these calculations, based on tight-binding molecular-dynamic techniques, were only performed for a limited number of angular directions, and the knock-on cross section was then only estimated on the basis of an isotropic potential well estimated at different atom positions around the tube circumference. They concluded that for 800 keV electrons, knock-on displacements are two to three times more common for carbon atoms located on the front and back side of the tube than for carbon atoms located at the wall side.

More recently, Smith and Luzzi,[10] taking into account a more complex scattering geometry, have shown that the threshold energy of the incident electron required to generate a knock-on carbon atom depends on the position of the carbon atom around the nanotube circumference. A minimum incident energy of 86 keV is required to remove carbon atoms from the tube section perpendicular to the electron beam. Higher energies exceeding 139 keV were estimated in order to generate knock-on carbon atoms from the tube wall section parallel to the beam. Nevertheless, the displacement energies were strongly approximated in their calculations and no local emission probabilities were calculated.

Despite the large interest shown in recent years for nanotube electron irradiation, a complete description of the sputtering cross section is still missing. In the present paper, we will derive the total knock-on cross section as a function of the atom position along the tube circumference. Furthermore, the knock-on cross section obtained for different electron beam energies will be presented for carbon and boron nitride nanotubes. The present paper is divided into four sections. After this short introduction, we illustrate in Sec. II the

theory of the knock-on process and of the scattering geometry. In Sec. III we derive through extended molecular-dynamics simulations the anisotropy of the emission energy threshold in a graphitic layer and a *h*-BN layer. Finally, in Sec. IV we report the total knock-on cross section for carbon and boron nitride single-walled nanotubes.

II. THEORY

Irradiation of electrons in matter can induce atom displacement, either through radiolytic processes related to electron excitation and ionization, or through direct knock-on collisions with the nuclei. Due to the delocalization of excitations in metals or small gap semiconductors, deexcitations are not translated into single atom energy transfer, and radiolysis cannot occur. Thus, since pure carbon nanotubes are metals or small gap semiconductors, we can assume that under irradiation, defects appear mostly through direct knock-on collisions.

The theoretical cross section for Coulomb scattering between a relativistic electron and a nucleus has been derived by Mott[11,12] as a solution of the Dirac equation. McKinley and Feshbach expanded the original Mott series in a power series[13] obtaining an approximate formula accurate up to the middle Z elements,

$$\sigma(\theta) = \sigma_R\left[1 - \beta^2 \sin^2 \theta/2 + \pi\frac{Ze^2}{\hbar c}\beta \sin \theta/2(1 - \sin \theta/2)\right], \tag{1}$$

where $\beta = v/c$, θ is the electron scattering angle, and σ_R is the classical Rutherford scattering cross section,

$$\sigma_R = \left(\frac{Ze^2}{4\pi\varepsilon_0 2m_0c^2}\right)^2 \frac{1-\beta^2}{\beta^4} \csc^4 \theta/2. \tag{2}$$

Under the approximation of pure elastic collisions, the maximum energy transfer T_{max}, corresponding to a scattering angle $\theta = \pi$, can be written as

$$T_{max} = \frac{2ME(E + 2mc^2)}{(M+m)^2c^2 + 2ME}, \tag{3}$$

where m is the electron mass, M the atom mass, and E the energy of the incident electron. The angular dependence on the scattering angle θ of the transferred energy to the atom is then expressed as

$$T(\theta) = T_{max} \sin^2(\theta/2). \tag{4}$$

Considering this notation, Eq. (1) can then be rewritten, after a few algebraic steps, as a function of the emission energy T,

$$\sigma(T) = \left(\frac{Ze^2}{4\pi\varepsilon_0 2m_0c^2}\frac{T_{max}}{T}\right)^2 \frac{1-\beta^2}{\beta^4}\left[1 - \beta^2\frac{T}{T_{max}} + \pi\frac{Ze^2}{\hbar c}\beta\left(\sqrt{\frac{T}{T_{max}}} - \frac{T}{T_{max}}\right)\right]. \tag{5}$$

In a monatomic gas, all the energy transferred from the electron to the atom is converted into kinetic energy. It is rather similar for an atom in a crystalline system if the transferred energy is much higher than the bonding energy of the atom. However, if the transferred energy is of the same order of magnitude as the bonding energy, the interaction between the knocked atom and its neighbors should be explicitly taken into account. Then, a simple model is usually assumed whereby damage can occur if the transfer of energy between the electron and the atom is larger than an emitting energy threshold E_d. For a transferred energy below the emitting energy threshold, the energy absorbed by the atom is converted into vibrational energy of the lattice.

To interpret experimental irradiation, the important quantity to consider is the total displacement cross section. It can be obtained by integrating the cross section of Eq. (5) inside the energy domain S over which emission conditions are satisfied,

$$\sigma_d = \int_{S(T>E_d)} \sigma(T)\frac{4\pi}{T_{max}}dT. \tag{6}$$

Despite the fact that crystalline solids usually have preferential directions for atom emission, E_d has been considered in many cases as an isotropic function. Under this hypothesis, Seitz and Koehler[14] have derived the following formula for the emission cross section:

$$\sigma_d = 4\pi\left(\frac{Ze^2}{4\pi\varepsilon_0 2m_0c^2}\right)^2 \frac{1-\beta^2}{\beta^4}\left\{\frac{T_m}{E_d} - 1 - \beta^2 \ln\left(\frac{T_m}{E_d}\right) + \pi\frac{Ze^2}{\hbar c}\beta\left[2\left(\frac{T_m}{E_d}\right)^{1/2} - \ln\left(\frac{T_m}{E_d}\right) - 2\right]\right\}. \tag{7}$$

Equation (7) can be useful to evaluate the total knock-on cross section.[8,9] Nevertheless, this approximation is not valid for strongly anisotropic systems where an angular dependence of the emission energy threshold occurs. In this case it is necessary to explicitly consider the emission energy threshold as a function of the emission angle and to integrate numerically Eq. (6) after having derived the correct integration energy domain S.

In Fig. 1(a) the scattering geometry during the irradiation process is represented for a layered material such as a graphene sheet. We consider an atom sitting in the center of the referential. The layer of material lies in the XY plane. $\vec{e}$, the incidence direction of the electron, lies within the XY plane at an angle α to Z, defined as the normal to the layer of material. It is then possible to describe the emission energy threshold for an atom emitted along an arbitrary direction $\vec{v}$ as a function of $E_d(\delta, \gamma)$, whose direction is defined in polar coordinates in terms of the polar angle δ and azimuthal angle γ.

We call Ω the emission angle defined by the angle between the electron incidence direction $\vec{e}$ and the atom emission vector $\vec{v}$. We can then rewrite Eq. (4) as a function of the emission angle Ω instead of the scattering angle θ, obtaining

$$T = T_{max} \cos^2(\Omega). \tag{8}$$

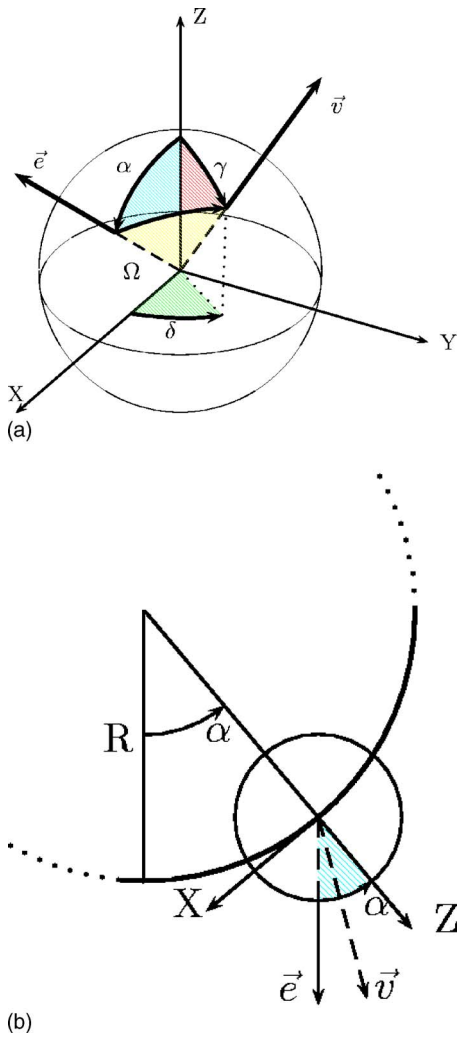

FIG. 1. (Color online) (a) Schematic representation of the irradiation geometry for a layered structure lying in the *XY* plane. The target atom sits at the center of the referential. $\vec{v}$ is atom emission direction and $\vec{e}$ is the incidence direction of the electron lying in the *XZ* plane. (b) Schematic representation of the irradiation geometry for a carbon nanotube, radius *R*, projected onto the *XZ* plane. The nanotube has its axis along *Y* perpendicular to the incident electron beam. The projection of $\vec{v}$ is represented as a dashed vector in this figure, although we note that in the general geometry assumed in our calculation the direction of the emitted atom $\vec{v}$ is not confined to the *XZ* plane.

The total knock-on cross section σ_d is then obtained by integrating Eq. (5) within the energy domain *S* for which the emission conditions are satisfied, i.e.,

$$T_{max}\cos^2(\Omega) \geqslant E_d(\delta,\gamma). \tag{9}$$

Transmission electron microscopy experiments are usually performed with nanotubes deposited onto a lacey carbon grid placed perpendicular to the TEM axis. Electron irradiation is then primarily performed in a nontilted case where the tube axis lies perpendicular to the direction of the electron beam. In this configuration, the position of the atoms around the tube circumference can be identified using the angle α defined by the direction of incidence of the electron and the local normal *Z* to the tube wall [see Fig. 1(b)]. If the tube diameter is large enough the structure can locally be considered as equivalent to a single graphene sheet. As described earlier with the irradiation geometry, the emission energy threshold function $E_d(\delta,\gamma)$ shows a dependence on the polar angle δ and the azimuthal angle γ. Nevertheless, this dependence disappears during the calculation of Eq. (6) since these two angles define the integration domain, and the total knock-on cross section σ_d only depends on the angle α and the value of the incident electron energy *E*. We can then define a function $\sigma_d(\alpha,E)$ that gives the total knock-on cross section for each atom of the nanotube as a function of the incident electron energy and its angular position α around the tube circumference.

III. EMISSION ENERGY THRESHOLD ANISOTROPY

A. Computational method

The characteristic time of interaction of a relativistic electron with a nucleus is several orders of magnitude lower than the time of emission of the atom. The interaction of the electron with the atom can thus be reasonably considered as a punctual event. Under this hypothesis, the ejection mechanism can be obtained through the time evolution of the total system after an initial energy *T* has been transferred to the knocked atom. The ejection is achieved when the initial energy is sufficient to extract the atom from the plane. To map this emission energy threshold including the local anisotropy $E_d(\delta,\gamma)$, we have adopted a molecular dynamics approach in a canonical ensemble. Energetics and forces have been computed within the framework of the density-functional tight-binding theory[15,16] (DFTB) as implemented in the DEMON2K code.[17] The DFTB technique is an ideal tool for these extended molecular dynamics calculations, since phenomena far from equilibrium can be described with the accuracy of a quantum method, while the benefit of the reduced computational cost of TB-based techniques is kept. This approach has been used by Krasheninnikov *et al.*[18] and by Loponen *et al.*[19] to calculate the radial emission of atoms in carbon nanotubes and nitrogen-doped carbon nanotubes. The radial emission condition gives the minimum emission energy threshold but in our calculation the whole emission energy threshold function is needed.

We first derive speeds and positions of all the atoms, equilibrating the system by molecular dynamics at a temperature of 300 K. In a second step, we simulate the knock-on process changing progressively the momentum of one of the atoms. For a fixed emission direction defined by the angles δ and γ, we perform a series of molecular-dynamics simulations varying the initial speed of the scattered atom in steps of 0.002 Å/fs until we reach the speed at which the atom is emitted. The characteristic time for an atom to escape from the system is few tenths of femtoseconds. Molecular-dynamic simulations are performed for a total time of 150 fs. When the final position of the scattered atom is more than 5 Å far from its initial equilibrium position, we consider that the atom is freestanding and that the initial momentum is above the emission threshold. We have followed this procedure for a carbon atom in a graphene

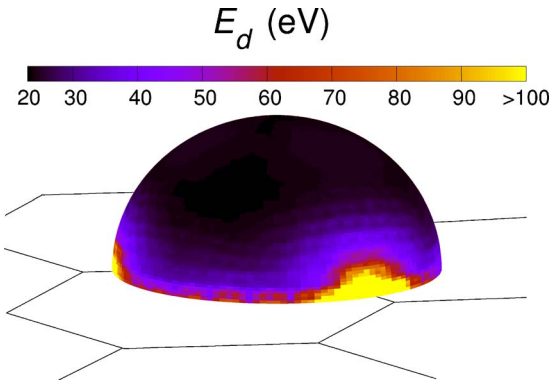

FIG. 2. (Color online) Three-dimensional representation of the map of the emission threshold function $E_d(\delta,\gamma)$ for a carbon atom in a graphitic layer as a function of the spherical coordinates δ and γ. The color scale indicates the emission energy values from 20 eV to more than 100 eV. The sphere indicates the emission direction for the ejected carbon atom. The sphere is centered on the initial position of the targeted C atom.

plane, as well as for boron and nitrogen atoms in a *h*-BN layer. Calculations have been performed using periodic boundaries conditions in a 7×7 supercell; test calculations with larger supercells give similar results for the emission energy threshold. In order to obtain a map of the emission energy threshold $E_d(\delta,\gamma)$, the total procedure is then repeated for a large set of angles δ and γ describing a total of 526 nonequivalent emission directions. A finer angular mesh is then obtained by a linear interpolation of the DFTB calculated energies. Finally, this mesh is used in the numerical integration of the total cross section to obtain the $\sigma_d(\alpha,E)$ which are discussed in Sec. IV.

B. Results

The map of anisotropy of the emission energy threshold, $E_d(\delta,\gamma)$, for a carbon atom in a graphitic layer is given in Fig. 2. Table I gives numerical values for specific angles. E_d shows little significant variance except for emission angles close to the plane.

TABLE I. Calculated emission energy threshold for a carbon atom in a graphene sheet and for a boron and nitrogen atom in a *h*-BN sheet as a function of different sets of the spherical angles γ and δ.

	γ (deg)	δ (deg)	E_d (eV)
Carbon	0	0	23
	90	0	780
	90	60	43
BN sheet: B atom	0	0	15
	90	0	90
	90	60	29
BN sheet: N atom	0	0	14
	90	0	234
	90	60	27

The minimum value of E_d is 23 eV, for emission orthogonal to the plane (γ=0). For initial momenta imparted within the graphene plane, i.e., γ=90°, E_d shows a strong dependence on the angle δ. Initial nucleus momentum toward a hexagon center (γ=0, δ=60) gives E_d of 43 eV. However, initial momentum in the direction of a nearest-neighbor atom (γ=0, δ=0) induces a large distortion of the lattice during the ejection process and thus high kinetic energies of the knocked atom, E_d up to 780 eV, are necessary for emission.

As discussed in Sec. II, irradiation defects can be produced when the transferred energy of an electron collision is larger than the displacement energy of an atom, i.e., T_{max} must be greater than $\min[E_d(\delta,\gamma)]$ for knock-on processes to occur. Equation (3), relating the T_{max} and the velocity of the incident electron, can then be used, after inversion, to estimate the minimum electron energy needed to sputter an atom. In the case of a carbon atom in a graphene plane, we found by DFTB that $\min[E_d(\delta,\gamma)]$=23 eV implies an electron beam energy threshold of 113 keV.

Smith and Luzzi[10] have experimentally demonstrated by changing the accelerating voltage on a TEM that the electron energy threshold for damaging single-walled carbon nanotubes lies between 80 and 100 keV. More accurate values are not available in the literature, but 100 keV seems to be nonetheless regarded as the upper limit by other authors.[20] Thus, the present DFTB calculations appear to overestimate the electron energy threshold by around 10–20% which corresponds to an overestimation of the atom emission energy threshold of around 2–4 eV. As has been demonstrated by Krasheninnikov *et al.*[18] curvature and chirality can reduce the emission energy threshold by a few eV. For a tube diameter of 10 Å, the threshold energy is 20.5 eV for an armchair tube and 18 eV for a zigzag tube. These energies increase with increasing diameter, tending asynthotically to the limit of 23 eV for a graphene plane. Another possible cause of the overestimation of the theoretical emission energy threshold energies comes from considering the atom sputtering mechanism as a pure knock-on process without any beam-induced electronic excitations. Their effect, as for radiolytic phenomena, is to reduce the bonding energy between the knocked atom and the lattice, in turn, reducing the kinetic energy necessary for atom emission. However, molecular-dynamics simulations based on DFT consider the ground-state electronic wave function and are not able to reproduce any coupling between the dynamical matrix and electronic excitations. A corrective term could be derived from a precise experimental measurement of the electron energy at which irradiation-induced defects start to appear. However, it is preferable to consider slightly overestimated values for the emission energy threshold derived from pure DFT-based molecular-dynamics simulation instead of adding any corrective term derived from the available experimental values which are only known with low accuracy.

Similarly to the case of a graphene sheet, we have derived $E_d(\gamma,\delta)$ for a boron and a nitrogen atom in a *h*-BN plane. The global trend of E_d is comparable with the results obtained for graphene. Table I gives E_d for different values of the angles γ and δ. There is a small difference, less than

1 eV, between the most favorable emission energy $E_d(0,0)$ for boron and nitrogen. This corresponds to the small difference in formation energy for the vacancies: boron and nitrogen vacancies in planar *h*-BN have formation energies of 11.22 and 8.91 eV,[5] respectively. However, the atomic mass dependence of the transmitted energy [see Eq. (3)] results in a different threshold for the electron beam energy at which atom emission occurs. A beam energy of 74 keV corresponds to a maximum energy transfer of 15 eV for a boron atom and the emission conditions are satisfied. However, for the same beam energy, the maximum energy transferred to a nitrogen atom is only 11.6 eV, lower than the minimum emission energy threshold. Emission conditions for nitrogen are only satisfied by increasing the incident electron energy to 84 keV. Thus, for beam energies between 74 and 84 keV, emission conditions are only satisfied for boron atoms, whereas above 84 keV, nitrogen atoms can also be sputtered. No accurate experimental data are available on electron irradiation in *h*-BN-based systems but as for the case of carbon we can suppose that our values for the atom emission energy thresholds in boron nitride are slightly overestimated due the curvature and induced electron excitation effects. This second effect should be stronger in *h*-BN than in carbon due to the partial ionic character of the BN bonding and the wide band gap of this material, which results in stronger localization of electron excitations.[21]

It is important to bear in mind that these results have been obtained for perfect graphene and hexagonal BN sheets; however, after some irradiation, a certain number of single vacancies will be present in the system. For vacancies in both graphite and *h*-BN, the first neighboring atoms have a lower coordination; the vacancy in graphite induces a Jahn-Teller distortion forming a weak C-C bond between two of the vacancy neighbors,[22] whereas in BN sheets there is no local reconstruction of dangling bonds.[5] During sputtering of an atom neighboring a vacancy, two bonds break instead of three for a fully coordinated atom. The case of a carbon nanotube has been treated in the works of Crespi *et al.*[9] and Krashenninikov *et al.*,[18] where the minimum of E_d for an (8,8) armchair nanotube was shown to drop from 20 to 14 eV. In the case of boron nitride nanotubes, we expect a similar lowering of the minimum electron beam energy at which atoms are sputtered, related to the reduced formation energy of vacancies neighboring a preexisting vacancy.[5] In this context, we can suppose that irradiating a BN nanotube with a beam energy between 74 and 84 keV will first generate a boron vacancy, but once these primary defects are created, nitrogen atoms on neighboring sites can also be emitted.

IV. TOTAL KNOCK-ON CROSS SECTIONS

A. Carbon nanotubes

In the previous section, we mapped the emission energy threshold for a carbon atom in a graphene layer. These results can be used to evaluate the cross section in the case of carbon nanotubes. The energy domain of integration S of the knock-on cross section $\sigma(T)$ in Eq. (6) has to be derived as a function of the angle α defining the position of the atom around the tube circumference. In the case of a nontilted nanotube imaged within a TEM, key angles are those corresponding to atoms located in tube region perpendicular ($\alpha=0°$) and parallel ($\alpha=90°$) to the incoming electron beam. We refer to these general orientations hereafter as the tube base (applying equally to the top and bottom tube surface) and tube sides, respectively.

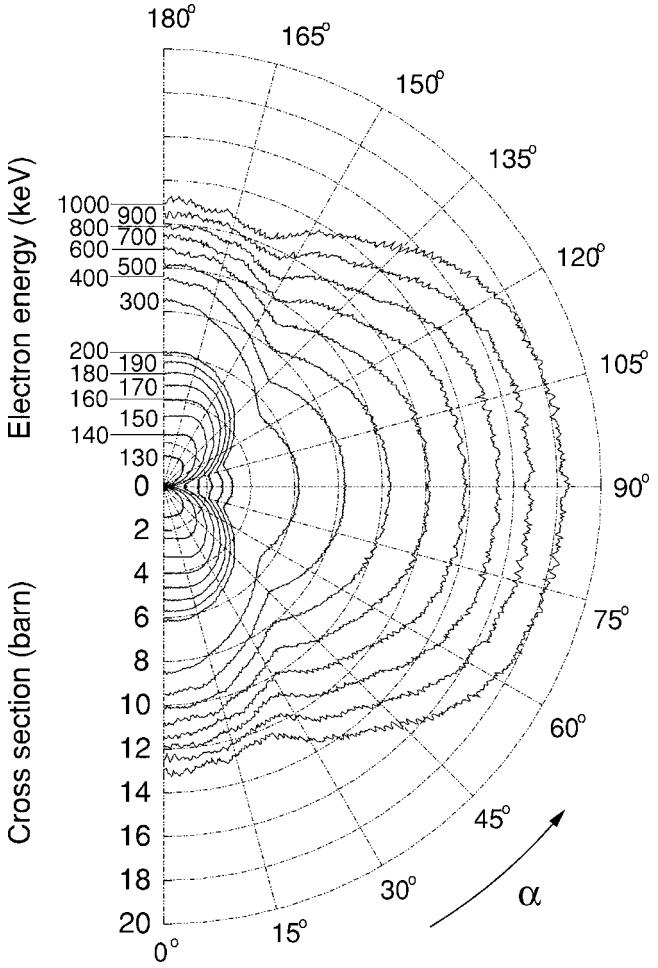

FIG. 3. Total knock-on cross section for carbon atoms in a single-walled carbon nanotube as a function of their position α around the tube circumference. Angles $\alpha=0°$ and $\alpha=90°$ refer, respectively, to carbon atoms in the tube base and in the tube side. The electron beam is entering vertically from the top of the figure. Total cross section for the full tube ($0° < \alpha < 360°$) can be obtained by symmetrization of the plot. The curves are plotted for incident electron energies between 130 keV and 1 MeV representative of the voltages used in TEM.

The total knock-on cross section σ_d for a carbon atom in a single-walled nanotube is plotted in Fig. 3 as a function of the polar angle α for different values of the incident electron energy in the range of 100 keV–1 MeV. The small high-frequency fluctuations on the curves is due to numerical noise introduced by the reduced sampling in the integration routine.

Since $\min(E_d)=23$ eV, tubes are theoretically predicted to be stable under electron irradiation with beam energies below 113 keV. Between 120 and 150 keV, atoms from the

tube base can be emitted. For example, at 130 keV, α values in the ranges of $-80° - +80°$ and $100° - +260°$ have nonzero cross sections. For an energy of 150 keV, there are no more forbidden regions for the knock-on process and all the atoms of the tube can be emitted. The maximum cross section is 3.5 barn corresponding to $\alpha=22°$ and to the three other symmetrically equivalent positions. At this energy, atoms in the tube base have higher sputtering probability than those in the tube walls where cross sections are still around 1 barn. This difference decreases with increasing incident electron energy, and for energies of a few hundred keV, emission is largely homogeneous around the tube circumference. For example, at 300 keV the cross section varies between 5.5 barn at $\alpha=54°$ and 8.5 barn at $\alpha=0°$. At higher irradiation energies, atom emission from the tube walls becomes more favorable: at 1 MeV the total cross section is 13.3 barn for $\alpha=0°$, 12.6 barn for $\alpha=22°$, and 16.5 barn for $\alpha=90°$. This may initially appear counterintuitive, since sidewalls are usually regarded as low probability sites for knock-on processes, even with high incident electron energy.[9] We will discuss this point in more detail in Sec. IV C.

In a previous work,[23] the total knock-on cross section for an electron beam energy of 300 keV was theoretically estimated to be 30 barn, within the approximation of an isotropic emission energy threshold equal to 15 eV. Crespi *et al.*[9] applying a similar hypothesis also mention cross sections from 10 to 50 bar. These values are generally higher than those we obtain here, and the difference shows the importance of explicitly considering the anisotropy of the function E_d. Several knock-on cross sections have been reported experimentally for carbon nanotubes and nanohorns. In both the paper of Hashimoto *et al.*[4] and Yuzvinsky *et al.*,[20] a cross section of 160 barn is reported, derived by a rough estimation of the quantity of sputtered material as a function of irradiation time. Hashimoto *et al.* observed defect density obtained by a limited dose irradiation at 120 keV. Yuzvinsky *et al.* investigated nanotube diameter shrinkage under higher irradiation doses at 100 keV; they derive then an extremely low value for the average emission energy threshold, estimated at 5.5 eV.

The small theoretical overestimation of the emission energy threshold E_d for a flat graphene plane compared to a locally curved one, previously discussed, cannot account for this difference in the total knock-on cross section. Indeed, tests we conducted by arbitrarily shifting the function E_d by 2–4 eV caused a variation in the corresponding total knock-on cross section of just a few barns. The large difference between experimental and theoretical cross sections primarily comes from the difficulty of precisely estimating experimentally the loss of matter after a certain irradiation time from which cross sections can successively be derived. Furthermore, the cross section measured via the carbon sputtering rate will be overestimated because after the creation of primary vacancies, any further sputtering events have a larger probability of occurring for atoms neighboring these preexisting vacancies. This behavior can be deduced by the reduction of neighboring vacancy formation energies resulting in the formation of a dislocation line.[5,24]

Our calculated cross sections for knock-on processes are primarily useful to estimate the amount of vacancies for low irradiation intensities or to estimate the average dose for a first vacancy to be created. Dynamics involving larger changes of the tube structure such as tube collapses cannot be simply understood by the knowledge of the knock-on cross section for a perfect tubular system.

Once atoms are removed from their position in the lattice, they can be ejected from the tube or emitted inside the tube cavity; the relative probability of these two events depends on the location of the atoms around the tube. Since cascade effects are limited to high accelerating voltages,[8] at normal TEM operating voltages atoms emitted into the tube are trapped inside the tube cavity. In a recent work of Banhart *et al.*,[23] it was discussed how atoms trapped inside the tube can diffuse along the tube axis and eventually nucleate in amorphous agglomeration. During the diffusion process, atoms can also recombine with existing vacancies, reducing the total number of defective sites in the system. Experimental determinations of knock-on cross sections will also be altered by this effect, related to the complex dynamics of the sputtering processes.

B. BN nanotubes

Figures 4 and 5 represent the total knock-on cross sections, respectively, for a boron and a nitrogen atom in a single-walled BN nanotube as a function of their position α for different incident electron energies between 80 and 500 keV. In both cases, the overall behavior is similar to that for carbon.

As previously discussed, at beam energies below 74 keV perfect BN nanotubes are not damaged by electron irradiation, and between 74 and 84 keV only primary boron vacancies can be generated. Between 84 and 140 keV, the total knock-on cross section of a boron atom is always higher than that of nitrogen. For example, at an irradiation energy of 100 keV, the total cross section at $\alpha=0°$ is 11.1 barn for a boron atom and 8.9 barn for a nitrogen atom; at $\alpha=90°$ it is 4.1 barn for a boron atom, whereas nitrogen atoms cannot be emitted for $72° < \alpha < 109°$.

Between 140 and 300 keV, two regimes appear: on the tube base nitrogen sputtering becomes more favorable, while at the walls the total knock-on cross section is still higher for boron atoms. For example, at 190 keV, the boron knock-on cross section is higher than that of nitrogen for angles $56° < \alpha < 124°$. Above 300 keV, nitrogen sputtering is the most probable event for all atoms around the tube circumference. We note that, as for carbon, at high incident electron energy the preferential site for boron and nitrogen atom ejections becomes the tube walls, $\alpha=90°$, whereas at low irradiation energies it was the tube base, $\alpha=0°$.

C. Discussion

In the previous sections, we have shown how for carbon and BN nanotubes the location of preferential sites for atom emission depends on the electron-beam energy. Two regimes have been described: for low energies, atoms in tube sections perpendicular to the incident beam have the highest emission probability, while at high energy the cross section is maximum in sections parallel to the incident beam. To explain this

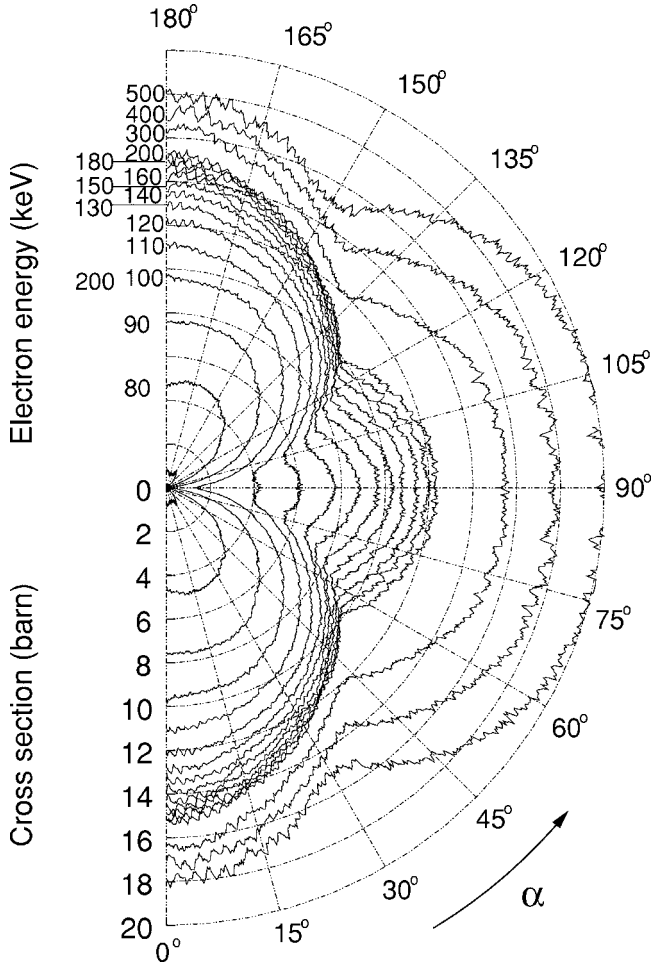

FIG. 4. Total knock-on cross section for boron atoms in a single-walled BN nanotube as function of their position α around the tube circumference.

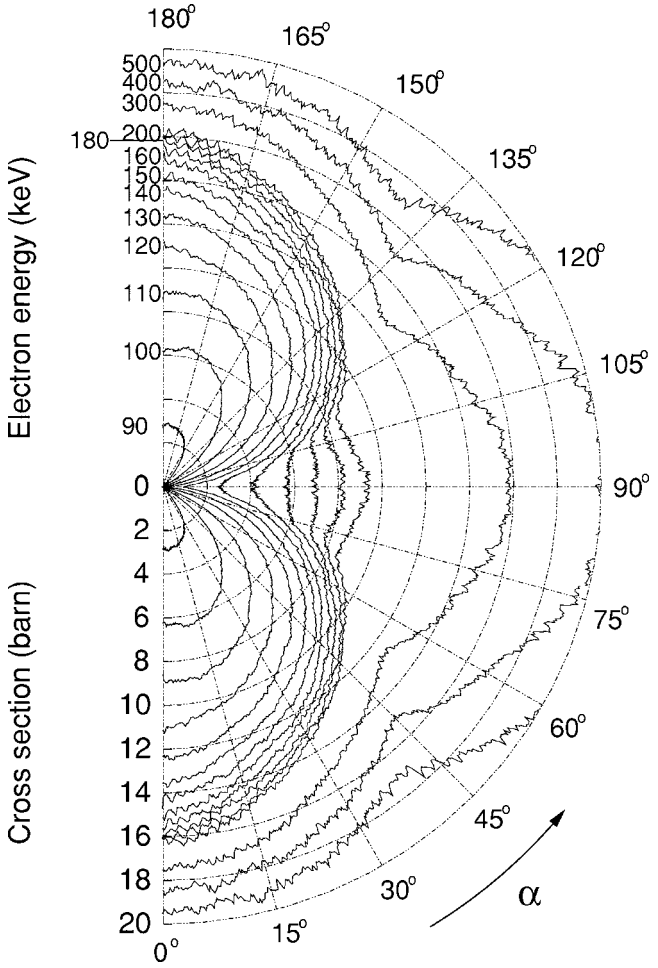

FIG. 5. Total knock-on cross section for nitrogen atoms in a single-walled BN nanotube as a function of their position α around the tube circumference.

behavior, we must consider the competition between the total integration domain S and the dependence on the transmitted energy T of the cross section $\sigma(T)$. We can clarify this point by examining in detail the solution of integral 6 in a simplified irradiation geometry. We consider here a simple two-dimensional case confining the atom emission direction Ω to lie in the XZ plane defined by the normal to the graphene sheet and the electron incidence direction (see Fig. 1).

Figure 6 shows this geometry for two different zones of tube, perpendicular to the electron beam ($\alpha=0°$) in the upper figure and parallel to the beam ($\alpha=90°$) in the lower. The three curves represent as a function of the emission angle Ω, the transmitted energy T (dashed line), the emission energy threshold E_d (dotted line), and the cross section $\sigma(T)$ (solid line). They have been calculated for an incident electron energy of 500 keV. In Table II we report the values of these three curves corresponding to different choices of the angle Ω.

As one can see in the dashed curves, a maximum energy transfer T_{max} of 136 eV is obtained at $\Omega=0°$ (i.e., when the atom is emitted parallel to the incoming electron beam) for an incident electron energy of 500 keV. Increasing Ω decreases the transferred energy [Eq. (4)], becoming 0 for $\Omega=90°$ (atom emission perpendicular to the incoming electron beam).

The E_d curves show two different behaviors. For $\alpha=0°$, the emission energy threshold has a minimum of 23 eV for $\Omega=0°$. E_d increases with Ω, almost diverging at $\Omega=90°$. This can be understood since in this configuration the plane is perpendicular to the incoming beam and at high $\Omega=90°$ atom emission is occurring parallel to the plane, an arrangement highly unfavorable for emission.

The situation is different for the E_d curve when $\alpha=90°$ (sheet parallel to the incoming electron beam). The function E_d is then rotated by 90° compared to the $\alpha=0°$ case. Thus, E_d reaches its maximum at $\Omega=0°$ (atoms emitted parallel to the sheet and incoming electron beam) and has a minimum equal to 23 eV for $\Omega=90°$ (atoms emitted orthogonal to the sheet and incoming electron beam). The knock-on cross section $\sigma(T)$ has been represented in Fig. 6 using a logarithmic scale. Independently from the plane orientation, this function has a strong dependence on Ω. It increases monotonically from a minimum of 0.08 barn at $\Omega=0°$ and diverges at $\Omega=90°$.

In Fig. 6 we have shaded the values of Ω for which the atom emission condition $T \geqslant E_d$ is satisfied. Due to the high-

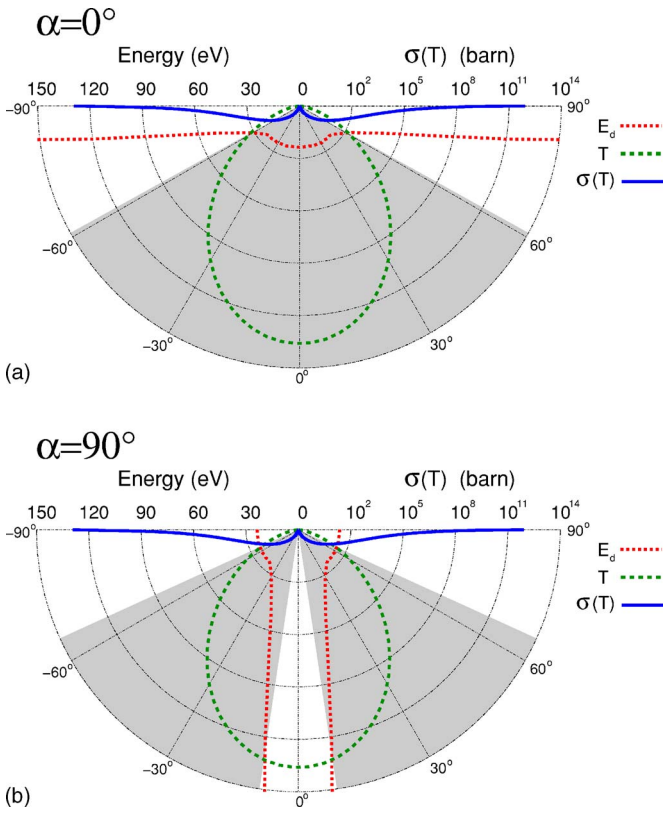

FIG. 6. (Color online) Transmitted energy T, emission energy threshold E_d, and cross section $\sigma(T)$ as a function of the emission angle Ω. The energy of the electron beam is 500 keV for both orientations $\alpha=0°$ (tube section perpendicular to the electron beam) and $\alpha=90°$ (tube section parallel to the electron beam).

symmetry values of α chosen, the integration regions are symmetric with respect to the electron incidence direction. For $\alpha=0°$ the emission region is defined as $|\Omega| \leqslant 61°$. Inside this region, the cross section σ varies between 0.08 barn for $\Omega_{min}=0°$ and 5.08 barn at $\Omega_{max}=61°$. For $\alpha=90°$, a higher value for $\Omega_{max}=65.5°$ is found, while at low angles there is now a forbidden zone within $|\Omega| \leqslant 8.5°$. In this case, σ is 10.0 barn at Ω_{max} and only 0.09 barn at Ω_{min}.

Comparing the two situations ($\alpha=0°$ and $\alpha=90°$), the difference in the total allowed emission angles Ω is small ($\Delta\Omega$ are 122° and 114°, respectively), showing larger geometrical possibilities for knock-on events in the case $\alpha=0°$. At first sight, this would appear to be in contradication with the previous finding where it was shown that the total cross section is highest in tube sections parallel to the beam ($\alpha=90°$) at 500 keV. However, the explanation is that the $\alpha=90°$ geometry allows knock-on cross sections with larger values of Ω (i.e., atom emission at angles further from the incident electron beam direction). It is precisely for such larger Ω values that the cross section rapidly increases (we remind the reader that cross section is plotted on a logarithmic scale in Fig. 6). In fact, although the energy threshold required to knock out atoms at low Ω values may be lower, such events have such small cross section that they do not contribute much to the total collision cross section when larger Ω values are also involved. This is the origin of the highest cross section for tube sections parallel to the incoming electron beam for high beam energies.

TABLE II. Transmitted energy T, emission energy threshold E_d, and cross section $\sigma(T)$ for different values of the emission angle Ω. The energy of the electron beam is 500 keV.

Ω	T (eV)	E_d (eV)		$\sigma(T)$ (barn)
		$\alpha=0°$	$\alpha=90°$	
0°	136	23	780	0.08
30°	102	24	30	0.27
60°	34	30	24	4.50
75°	9	69	24	71.82
90°	0	780	23	∞

V. CONCLUSIONS

In the present paper, we have derived, through extended DFTB-based molecular-dynamics simulations, the emission energy threshold map for a carbon atom in a graphene sheet and for boron and nitrogen atoms in an *h*-BN layer. In a successive step, we have obtained the total knock-on cross section for atoms in carbon and boron nitride nanotubes.

Previous theoretical studies have calculated the total knock on cross section using the approximation of atoms lying in an isotropic potential well. Under this hypothesis, cross sections are overestimated and it is not possible to obtain their dependence on the atomic position around the tube circumference. Including explicitly the anisotropy of the emission energy threshold, we have described a picture of the sputtering process, showing a strong dependence of the total cross section on the incident electron energy and the circumferential position of the atoms.

Two regimes are obtained: at low irradiation energies, atoms are preferentially ejected from the tube regions perpendicular to the incident electron beam at low emission angles, and at high energies from the tube regions parallel to the beam at high emission angles. This behavior can be explained through the competition between the angular dependence of the cross section and its range of integration. For BN nanotubes, we find an additional effect which promotes boron sputtering for low irradiation energies and nitrogen sputtering for high energies.

For all the energies and atom positions considered, the total cross section is below 20 barn, which is much lower than reported experimental values. The difficulty of clearly evaluating the total amount of sputtered atoms strongly affects experimentally derived cross sections. Furthermore, at high irradiation doses, large structural modifications occur and a model based on single vacancy formation is no longer valid. Vacancy formation energies are drastically reduced in the vicinity of other vacancies with a consequent increase in their sputtering probability. Under electron irradiation, this effect promotes the formation of defects based on extended lines of neighboring vacancies, through a "laddering" mechanism of the tube lattice.

The results presented in this paper may be helpful for the interpretation and design of future experiments. For low electron doses, irradiation experiments predominantly lead to single vacancy formation. Density and spatial distribution of vacancies around the tube circumference can then be directly obtained with the estimated total cross sections discussed above. At higher doses, the primary defects become seeds for the germination of more extended defects.[25] Although a full description for these higher electron doses would need to go beyond the single vacancy model presented here, our calculations can nonetheless be used to determine the threshold dose to initiate such extended defects. They may thus also be useful if, for example, one wants to shape the nanotube with an electron beam at high spatial resolution. Experiments are currently in progress using a dedicated scanning transmission electron microscope.

ACKNOWLEDGMENT

A.Z. would like to thank the New Fullerene-Like Materials Network, Contract No. HPRNCT-2002-00209, for financial support.

*Electronic address: zobelli@lps.u-psud.fr

[1] C. Gómez-Navarro, P. de Pablo, J. Gómez-Herrero, B. Biel, F. Garcia-Vidal, A. Rubio, and F. Flores, Nat. Mater. **4**, 534 (2005).
[2] B. Biel, F. J. García-Vidal, A. Rubio, and F. Flores, Phys. Rev. Lett. **95**, 266801 (2005).
[3] M. Sammalkorpi, A. Krasheninnikov, A. Kuronen, K. Nordlund, and K. Kaski, Phys. Rev. B **70**, 245416 (2004).
[4] A. Hashimoto, K. Suenaga, A. Gloter, K. Urita, and S. Iijima, Nature (London) **430**, 870 (2004).
[5] A. Zobelli, C. Ewels, A. Gloter, G. Seifert, O. Stephan, S. Csillag, and C. Colliex, Nano Lett. **6**, 1955 (2006).
[6] K. Urita, K. Suenaga, T. Sugai, H. Shinohara, and S. Iijima, Phys. Rev. Lett. **94**, 155502 (2005).
[7] F. Banhart, J. Mater. Sci. **41**, 4505 (2006).
[8] F. Banhart, Rep. Prog. Phys. **62**, 1181 (1999).
[9] V. H. Crespi, N. G. Chopra, M. L. Cohen, A. Zettl, and S. G. Louie, Phys. Rev. B **54**, 5927 (1996).
[10] B. Smith and D. Luzzi, J. Appl. Phys. **90**, 3509 (2001).
[11] N. Mott, Proc. R. Soc. London, Ser. A **124**, 426 (1929).
[12] N. Mott, Proc. R. Soc. London, Ser. A **135**, 429 (1932).
[13] W. McKinsley and H. Feshbach, Phys. Rev. **74**, 1759 (1948).
[14] F. Seitz and J. Koehler, *Solid State Physics* (Academic, New York, 1956), Vol. 2.
[15] D. Porezag, T. Frauenheim, T. Köhler, G. Seifert, and R. Kaschner, Phys. Rev. B **51**, 12947 (1995).
[16] G. Seifert, P. Fowler, D. Porezag, and T. Frauenheim, Chem. Phys. Lett. **268**, 352 (1997).
[17] A. Köster, R. Flores, G. Geudtner, A. Goursot, T. Heine, S. Patchkovskii, J. Reveles, A. Vela, and D. Salahub, DEMON 2004, NRC, Ottawa, Canada, 2004.
[18] A. V. Krasheninnikov, F. Banhart, J. X. Li, A. S. Foster, and R. M. Nieminen, Phys. Rev. B **72**, 125428 (2005).
[19] T. Loponen, A. V. Krasheninnikov, M. Kaukonen, and R. M. Nieminen, Phys. Rev. B **74**, 073409 (2006).
[20] T. Yuzvinsky, W. Mickelson, S. Aloni, G. Begtrup, A. Kis, and A. Zettl, Nano Lett. **6**, 2718 (2006).
[21] L. Wirtz, A. Marini, and A. Rubio, Phys. Rev. Lett. **96**, 126104 (2006).
[22] A. A. El-Barbary, R. H. Telling, C. P. Ewels, M. I. Heggie, and P. R. Briddon, Phys. Rev. B **68**, 144107 (2003).
[23] F. Banhart, J. X. Li, and A. V. Krasheninnikov, Phys. Rev. B **71**, 241408(R) (2005).
[24] J. Kotakoski, A. V. Krasheninnikov, and K. Nordlund, Phys. Rev. B **74**, 245420 (2006).
[25] J. Y. Huang, S. Chen, Z. F. Ren, Z. Q. Wang, D. Z. Wang, M. Vaziri, Z. Suo, G. Chen, and M. S. Dresselhaus, Phys. Rev. Lett. **97**, 075501 (2006).